Nanoscale

PAPER

View Article Online
View Journal | View Issue

Cite this: *Nanoscale*, 2026, **18**, 7461

A helical polydiacetylene with enhanced thermochromic reversibility temperature from self-assembly of diacetylene-containing rosettes

Hyemin Kang,†[a] Woomin Jeong,†[a] Mohammed Iqbal Khazi*[b] and Jong-Man Kim *[a,b]

Rosettes are a class of higher-order hierarchical supramolecular structures formed through highly precise and controlled molecularly coordinated self-assembly *via* sequential non-covalent interactions, predominantly directed by hydrogen-bonding networks. Herein, we constructed robust hydrogen-bonded colorimetric hexad rosette supramolecules through the self-assembly of linear barbituric acid-linked diacetylene monomers (PCDA-ABA). The barbituric acid head group, with multiple hydrogen-bond donor and acceptor sites, facilitates sequential packing, forming a cyclic hexameric rosette arrangement. These hexad rosettes stack along the axis in a columnar fashion, forming nanohelices stabilized by hydrogen bonding originating from the barbuteric acid moiety and π–π stacking interactions of the diacetylene (DA) chains. Interestingly, upon UV-induced photopolymerization, the columnar stacked rosettes transform into a rigid covalent structure, imparting distinct colorimetric properties to the resulting polymeric assemblies. Results from structural arrangement analysis using FT-IR indicate that hydrogen bonding is the major driving force behind the formation of hexad rosette nanohelices. Studies of structural packing patterns and morphological characteristics using XRD, AFM, SEM, and TEM strongly support the formation of rosette-based nanohelices. Photopolymerization results in a covalently linked blue-phase PDA rosette structure, which exhibits enhanced reversible thermochromic properties up to 180 °C over multiple thermal cycles. Also, the pH-dependent behavior of the self-assembled PDA was evaluated, revealing a reversible colorimetric response regulated by protonation and deprotonation processes.

Received 15th November 2025,
Accepted 1st March 2026

DOI: 10.1039/d5nr04836b

rsc.li/nanoscale

1. Introduction

Supramolecular structures self-assemble through weak non-covalent bonds, offering a feasible approach to creating functional materials with properties responsive to external stimuli.[1–5] These materials, which extend their functionality beyond individual molecules, rely on non-covalent interactions to form precise and ordered architectures.[1,6–12] In addition, the magnitude of these non-covalent interactions drives the functional performance of these materials. Among the vast array of functional materials developed, hydrogen bonding has served as a powerful tool to construct supramolecular assemblies due to its directionality, inherent tunability, and partial covalent character.[13–15] Supramolecular structures range from simple one-dimensional assemblies to higher-order two-dimensional or three-dimensional superstructures and morphologies, including nanotubes, toroids, and rosettes.[16–23] Of particular interest are rosettes, which represent distinct cyclic structures formed through directional non-covalent interactions such as hydrogen bonding, metal coordination, and π–π stacking. Exhibiting a flower-like geometry, rosettes typically consist of six monomeric units arranged into a planar hexamer stabilized by multiple hydrogen bonds. These cyclic assemblies can further stack, aggregate, or organize into higher-order one-, two-, or three-dimensional architectures, including complex structures such as double helices, nanotubes, or fibers.[24–26]

Polydiacetylenes (PDAs) are π-conjugated colorimetric polymers. PDAs are intrinsically supramolecular structures through the self-assembly of diacetylene (DA) monomers *via* non-covalent interactions.[27–32] Since weak non-covalent bonds stabilize PDA structures, PDAs have been widely used as stimuli-responsive functional materials. Typically blue in color, with an absorption band around 650 nm, PDAs undergo a distinct blue-to-red color transition when exposed to external stimuli. Due to their visible, naked-eye-detectable chromatic response, PDAs are extensively employed as sensing materials in various sensor systems.[33–41]

[a]*Department of Chemical Engineering, Hanyang University, Seoul 04763, Korea. E-mail: jmk@hanyang.ac.kr*
[b]*Institute of Nano Science and Technology, Hanyang University, Seoul 04763, Korea. E-mail: iqbal.khazi@gmail.com*
† These authors contributed equally to this work.

Many approaches for constructing rosettes have been previously reported;[24–26,42–44] however, rosette structures with complementary colorimetric properties for functional applications have not yet been explored. In this study, we integrated diacetylene monomers with the hydrogen-bonding motif barbituric acid to construct PDA-based colorimetric rosette superstructures (PCDA-BA) and investigated their supramolecular assemblies, morphological characteristics, and thermochromic properties. Barbituric acid serves as an intriguing non-covalent interaction-imparting motif during self-assembly.[45,46] Barbituric acid possess multiple hydrogen-bond donor and acceptor sites that enable diverse binding orientations "head–head" (HH), "head–shoulder" (HS), and "shoulder–shoulder" (SS), which form extended hydrogen-bonded networks leading to self-patterned, higher-order superstructures such as tapes, ribbons, and rosettes.[47–51] Hence, we anticipated that the barbituric acid head group in PCDA-BA would facilitate the helical packing of amphiphiles, resulting in the formation of higher-order hexameric rosette morphologies. The supramolecular PCDA-BA rosettes undergo UV-induced topochemical polymerization, resulting in a robust, covalently linked polymeric blue-phase PDA, P(PCDA-BA). Although PDAs have been extensively explored for their thermochromic properties, but the majority of reported systems exhibit irreversible thermochromism, with only a few showing reversible color transitions, typically stable up to about 150 °C.[20,52–57] Whereas the blue-phase rosette PDA, P(PCDA-BA), exhibited better colorimetric properties with enhanced thermochromic performance up to 180 °C, showing reversibility and repeatability over multiple thermal cycles.

2. Results and discussion

As shown in Fig. 1a, we constructed a barbituric acid-linked diacetylene monomer system (PCDA-ABA). A multistep synthetic protocol was employed, and the structures of all intermediates and the target molecule, PCDA-ABA, were characterized by NMR, MS, and FT-IR spectroscopic methods (see Scheme S1 and Fig. S1–S6 in the SI).

Barbituric acid, with multiple donor–acceptor hydrogen-bonding sites, could serve as a head-to-head self-assembly template, complemented by hydrogen bonding from the amide functionality in the DA chain and π–π stacking of the diacetylene moiety, to form a self-patterned hexad rosette structure. Fig. 1b illustrates the self-assembly of a hydrogen-bonded rosette through a sequence of intermolecular interactions to create linear supramolecular oligomers, followed by the intramolecular macrocyclization of six monomer units forming a hexad rosette assembly. These hexad rosettes tend to stack to form twisted slip-stacked supramolecular columnar structures, which are held together by hydrogen bonding of the amide groups and π–π stacking diacetylene template of the DA chains (Fig. 1c). Columnar stacked hexameric rosettes are primarily held together by weak non-covalent interactions. Upon UV irradiation, the stacked diacetylene moieties undergo photopolymerization, forming a highly robust, covalently linked structure with an extended conjugated backbone along the columnar axis, producing a blue-phase colorimetric rosette PDA with enhanced stability (Fig. 1d).

The self-assembly behavior of PCDA-ABA was investigated in tetrahydrofuran (THF) and THF/ethanol mixture. The morphological characteristics were initially examined using SEM and TEM, followed by AFM. To understand the influence of concentration and solvent polarity on morphology, we tested self-assembly by adjusting the polarity of the solvent using a THF : ethanol mixture and varying the concentration of PCDA-ABA to identify the ideal solvent and concentration values for fabricating rosette morphology. PCDA-ABA exhibited distinct morphological characteristics at varying concentrations of PCDA-ABA (1 mg mL^{-1}, 2 mg mL^{-1}, 10 mg mL^{-1}, and 20 mg mL^{-1}) in a THF : ethanol mixture (v/v) at a 1 : 12 ratio. The irregular granular-like structures observed at 1 mg mL^{-1} concentration (Fig. 2a) transform into plate-like structures at 2 mg mL^{-1} (Fig. 2b). An interesting twisted nanohelices morphology was observed at a concentration of 10 mg mL^{-1} (Fig. 2c). Upon further increasing the concentration to 20 mg mL^{-1}, PCDA-ABA self-assembles into densely packed twisted nanohelices (Fig. 2d).

Next, polarity optimization was performed by using varying THF : ethanol mixture ratios: 30 : 1, 12 : 1, 6 : 1, 1 : 1, 1 : 6, 1 : 12, and 1 : 30 (Fig. S7). Highly ordered twisted nanohelices were obtained in a THF : ethanol mixture at a ratio of 1 : 12 (v/v) with a concentration of 10 mg mL^{-1} (Fig. 3a).

The morphological transition from granular structures to nanoplates and ultimately to helical fibers is driven by solvent polarity-dependent self-assembly behavior. Increasing ethanol content gradually reduces solubility, thereby enhancing intermolecular hydrogen bonding and π–π interactions. At lower ethanol ratios, weak intermolecular association results in granular aggregates. With further ethanol addition, stronger directional interactions promote the formation of ordered nanoplates. At even higher ethanol fractions, cooperative stacking and packing anisotropy induce twisting, leading to the formation of helical fibers. A THF : ethanol mixture at a 1 : 12 (v/v) ratio with a concentration of 10 mg mL^{-1} was found to be optimal for nanohelices formation.

TEM imaging of self-assembled PCDA-ABA showed highly extended nanohelices, organized as both isolated individual nanofibers and dense aggregated arrays of bundled fibers (Fig. 3b). The helicity indicates a twist angle rotation of the PCDA-ABA rosette upon stacking, forming a columnar structure with a fibrous morphology. AFM imaging also revealed the formation of extended nanohelices (Fig. 3c). The nanohelices are observed to form through the overlap and intertwining of multiple strands. Measurements from the AFM micrograph indicate that the height of an individual strand is approximately 8–9 nm, while the thickness of helices formed by multiple strands ranges from 97 nm to 121 nm, as detailed in the inset graph. These measurements indicate the hierarchical assembly of PCDA-ABA, beginning at the molecular level with rosette structures and progressing to the formation of nanohelices through further aggregation. The observed strand height of 8–9 nm aligns well with

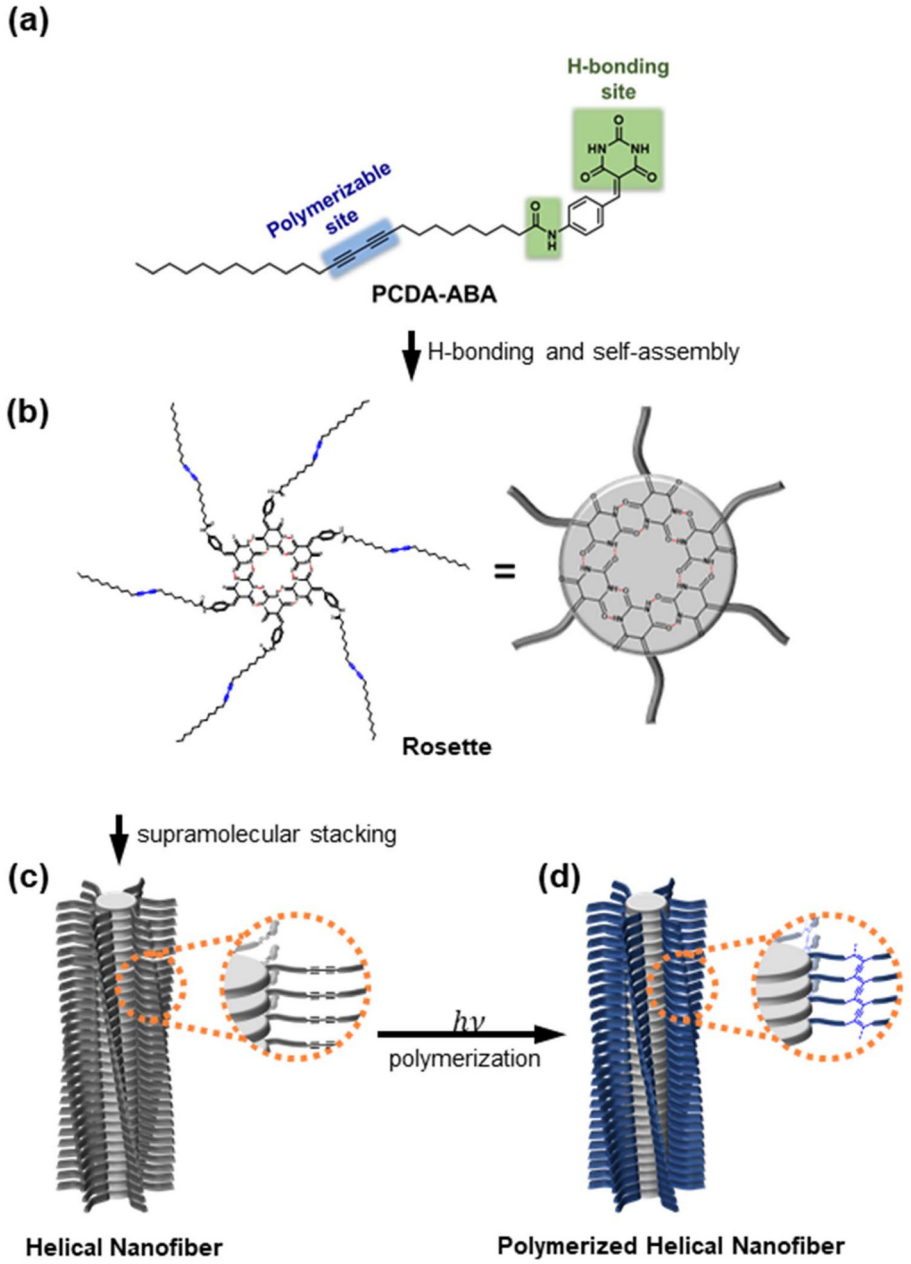

Fig. 1 Schematic representation of the formation of PCDA-ABA nanohelices. (a) Molecular structures of PCDA-ABA. (b) Self-assembly of PCDA-ABA *via* hydrogen bond. (c) Supramolecular stacking of PCDA-ABA and (d) formation of UV-induced covalently linked polymeric P(PCDA-ABA).

the previously calculated *d*-spacing of 7.2 nm from XRD analysis, which corresponds to the diameter of the rosette structure. This strongly supports the hypothesis that the individual strands observed in AFM result from the stacking of rosette structures driven by extensive hydrogen bonding interactions. The formation of nanohelices, exceeding 100 nm in thickness, suggests the hierarchical assembly of rosette-based strands. This organization is likely driven by van der Waals forces, π–π stacking, and directional hydrogen bonding of barbituric acid moieties. These findings demonstrate a two-step self-assembly of PCDA-ABA: (1) hydrogen-bonded rosette formation and (2) hierarchical assembly into nanohelices *via* cooperative strand interactions. AFM images confirm this organization, aligning with spectroscopic and diffraction data. Further, powder X-ray diffraction (PXRD) studies were conducted to analyze the packing patterns of PCDA-ABA rosettes (Fig. 3d). Diffraction peaks at 2.5°, 3.7°, 4.9°, 6.1°, 7.3°, 8.6°, and 9.8° for stacked hexameric rosettes (PCDA-ABA) with fully extended DA tails correspond to an intramolecular distance of 7.2 nm. Furthermore, the analysis also revealed hexad stacks with an interstack distance of 23.04 Å for the DA tails, which is optimal for the topochemical polymerization of diacetylene templates.

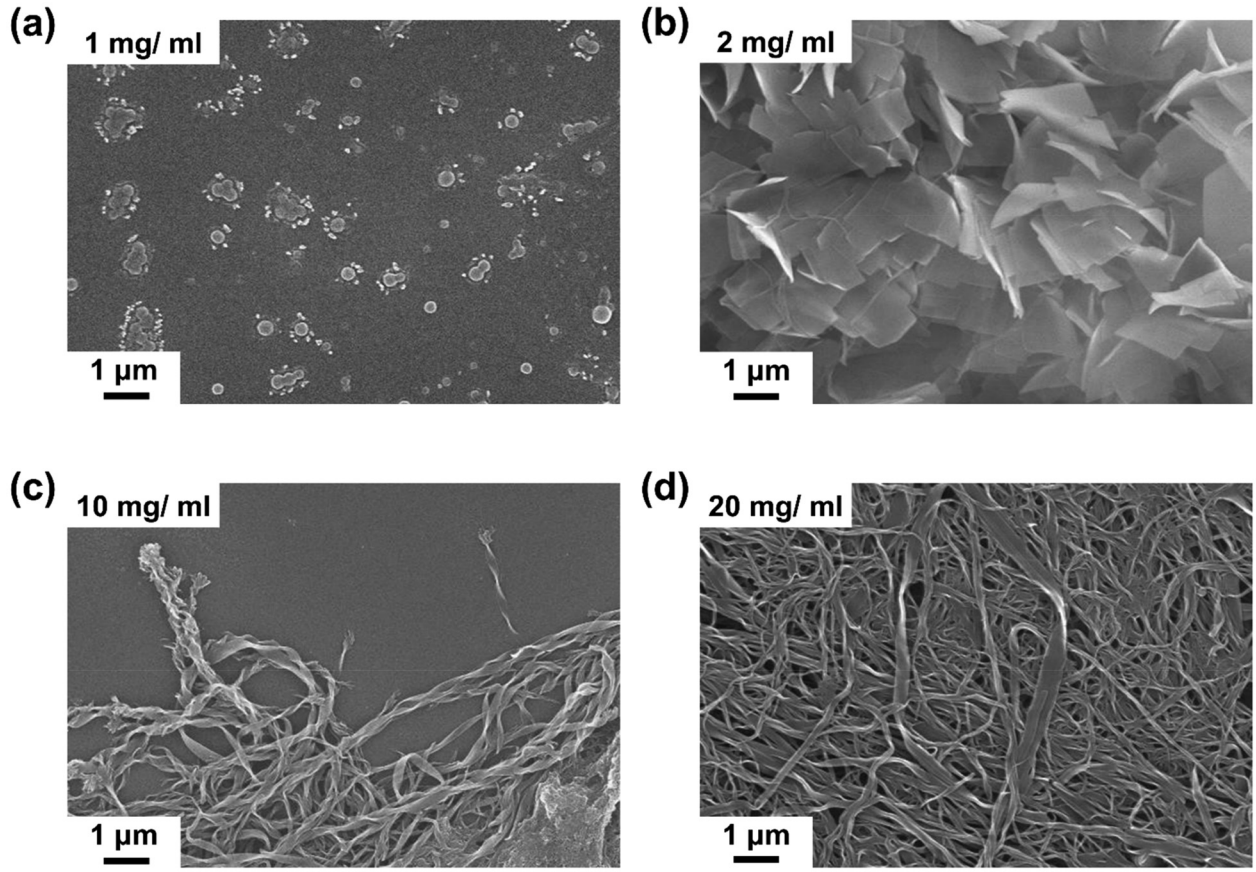

Fig. 2 SEM images of self-assembled PCDA-ABA, obtained with different concentrations in THF : ethanol mixture (v/v) at a 1 : 12 ratio. (a) 1 mg mL^{-1}. (b) 2 mg mL^{-1}. (c) 10 mg mL^{-1}. (d) 20 mg mL^{-1}.

FT-IR analysis (Fig. 4a) confirms hydrogen bonding in self-assembled PCDA-ABA. The N–H stretching vibrations shift from 3384 cm^{-1} and 3320 cm^{-1} to 3281 cm^{-1} upon self-assembly, indicating hydrogen bond formation. Similarly, C═O stretching peaks shift from 1739 cm^{-1}, 1693 cm^{-1}, and 1672 cm^{-1} to 1769 cm^{-1}, 1741 cm^{-1}, and 1664 cm^{-1}, respectively. While the non-hydrogen-bonded carbonyl group shows minimal shift, the hydrogen-bonded carbonyls exhibit significant changes, confirming strong interactions. The amide carbonyl group (gray star) shows a minor shift, indicating limited involvement in the hydrogen-bonding network. The observed spectral shift patterns confirm the presence of a strong hydrogen-bonded network, supporting the formation of a highly organized rosette structure. Based on collective information obtained from PXRD and FT-IR analyses, a schematic illustration of PCDA-ABA self-assembly into hexad rosettes is shown in Fig. 4b. The packing of PCDA-ABA hexad rosette stacks exhibits a twist angle rotation. From the collective results, FT-IR and XRD data, a schematic representation of PCDA-ABA nanohelices is illustrated, highlighting the hierarchical organization facilitated by hydrogen bonding (Fig. 4b). The shifts in N–H and C═O stretching vibrations confirm extensive hydrogen bonding, while the 7.2 nm intramolecular distance observed in XRD strongly suggests the helical packing of PCDA-ABA rosette structures. The correlation between spectral shifts, peak broadening, intensity variations in FT-IR, and periodic diffraction patterns in XRD provides strong evidence that barbituric acid participates in extensive, directional hydrogen bonding, leading to a highly organized self-assembled rosette structure.

Next, the columnar stacks of PCDA-ABA hexad rosettes are covalently integrated through UV-induced topochemical polymerization. Upon UV irradiation (254 nm, 10 s), the white color PCDA-ABA rosettes transform into a brilliant blue color (displayed as an inset in Fig. 5a), indicating effective polymerization and the formation of an extended π-conjugated PDA structure along the columnar axis. The formation of PDA was confirmed through UV-vis and Raman spectroscopy. In the UV-vis spectrum, an absorption maximum peak at 615 nm appeared in the visible region, confirming the formation of the conjugated ene–yne PDA chain (a). Further confirmation of PDA formation was provided by Raman spectroscopy. The characteristic bands associated with the conjugated ene–yne structure in the PDA phase appeared at 1460 cm^{-1} (C═C) and 2099 cm^{-1} (C≡C), while the band corresponding to the monomer yne–yne band at 2270 cm^{-1} (C≡C) nearly disappeared (Fig. 5b). Molecular weight of the polymer P(PCDA-ABA) could not be determined due to experimental

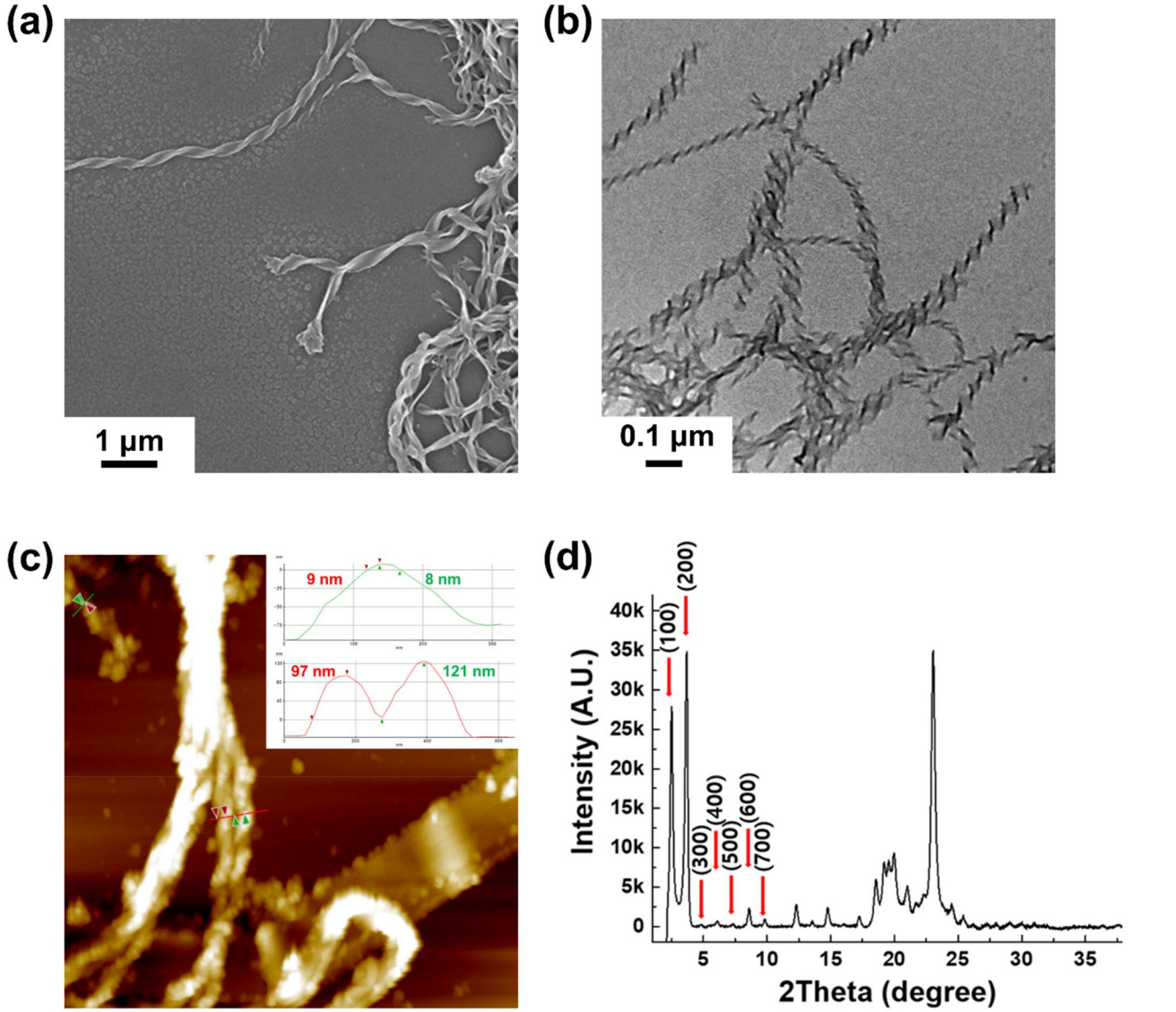

Fig. 3 (a) SEM and TEM (b) images of PCDA-ABA nanohelices, generated in mixed THF and EtOH solution (1 : 12 v/v). (c) AFM images of PCDA-ABA nanohelices. The inset image shows the thickness profiles of the corresponding to the section analyses shown in (c). (d) Powder XRD pattern of PCDA-ABA nanohelices.

limitations, primarily arising from poor solubility of the polymerized structure. However, based on theoretical calculations, the blue-phase PDA typically requires at least ~40 conjugated carbons (~10 diacetylene monomers) to absorb at 640 nm.[58] Also, the results of our previous studies have shown that the blue-phase PDAs have a molecular weight in the range of 30 000 to 200 000.[59,60] On this basis, it can be inferred that the topochemical polymerization to form the blue-phase PDA, P(PCDA-ABA), has proceeded efficiently, resulting in molecular weights in the range of 30 000–200 000.

Given that the blue-phase rosette PDAs can be easily prepared through facile UV irradiation, we tested their colorimetric response to heat to explore the possibility of devising thermochromic sensor systems. To examine the thermochromic behavior, the blue-phase P(PCDA-ABA) was gradually heated from 25 °C to 200 °C at a rate of 10 °C min^{-1} on a hot plate. P(PCDA-ABA) displayed a naked-eye visible, temperature-dependent color transition. As shown in Fig. 6a, the blue-phase PDA at room temperature undergoes heat-induced multiple color transitions. A blue-purple phase change occurs between heating temperatures of 70–90 °C, followed by a transformation into a sharp red phase at 100 °C, which is maintained up to 170 °C. Further heating results in a color change to orange between 180 °C and 200 °C. Most interestingly, the P(PCDA-ABA) exhibited excellent thermochromic reversibility. A reversible blue-to-red color transition occurred during repeated heating and cooling cycles between 25 °C and 180 °C, with complete recovery of the blue color (Fig. 6b, heating and cooling cycles are marked with an arrow).

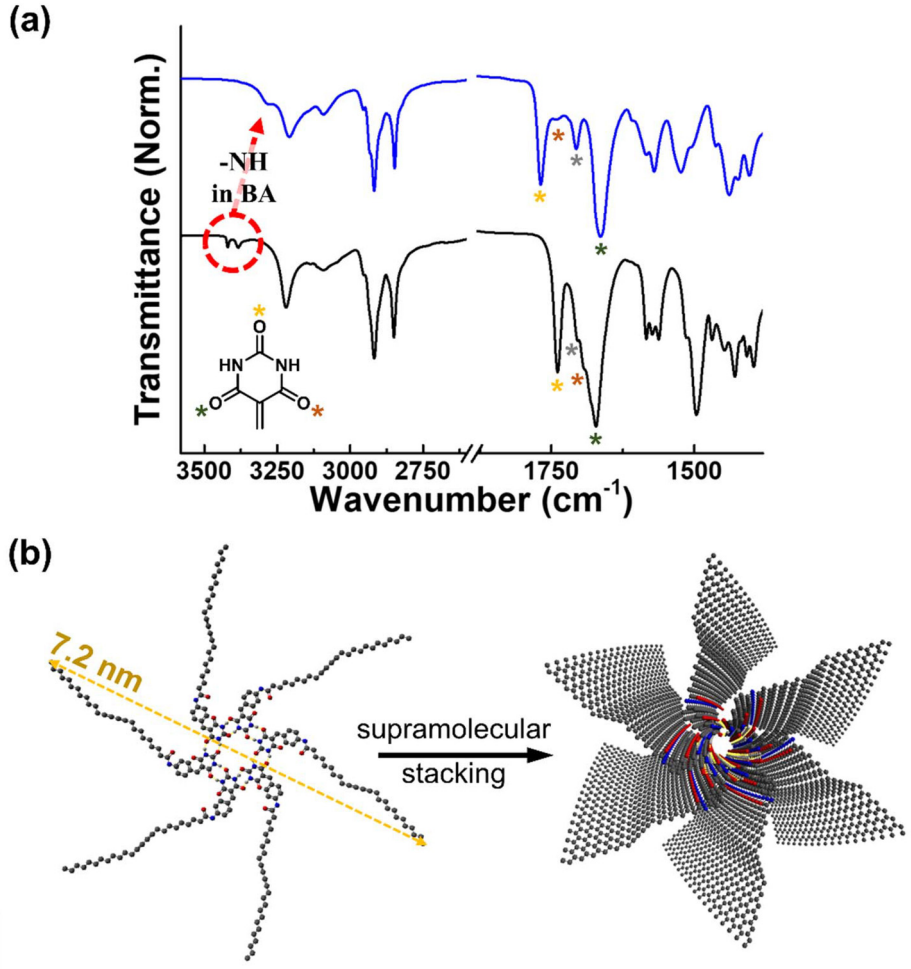

Fig. 4 (a) FT-IR spectra (C═O and N–H stretching region) of the PCDA-ABA (black line), PCDA-ABA nanohelices (blue line). (b) The proposed self-assembled structure of PCDA-ABA nanohelices and schematic representation of the self-assembly process. PCDA-ABA is first self-assembled into rosettes, followed by a gradual rotation and stacking process to ultimately form nanohelices.

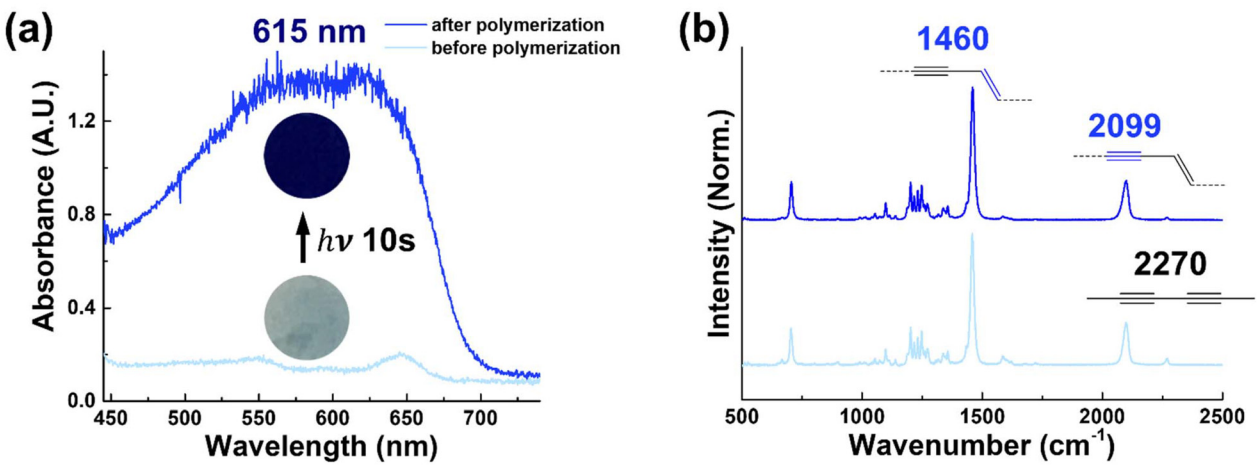

Fig. 5 (a) UV-vis and (b) Raman spectra of PCDA-ABA nanohelices before (sky-blue line) and after (blue line) UV irradiation. The inset photographs show monomeric (below) and polymeric (above) PCDA-ABA nanohelices.

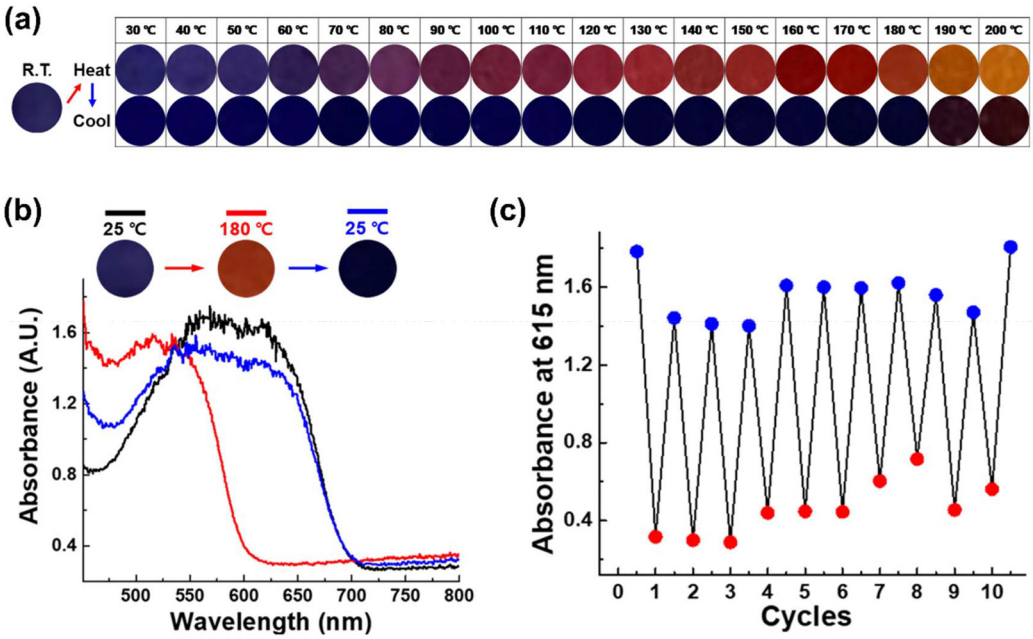

Fig. 6 (a) Digital images of thermochromic behaviour of polymerized PCDA-ABA nanohelices upon gradual heating from 25 °C to 200 °C. (b) UV-vis absorption spectra of polymerized PCDA-ABA before (black line), after heating at 180 °C (red line) and after cooling the sample back to 25 °C (blue line). (c) Plots of absorbance intensity at 615 nm as a function of thermal cycles (25 ↔ 180 °C).

The potential of the thermochromic sensory response of P(PCDA-ABA) for developing a reusable sensor system was evaluated by performing repeated consecutive thermal cycles. As shown in Fig. 6c, after multiple cycles of alternating heating and cooling, no noticeable change in the intensity of the absorption peak occurred, strongly indicating the excellent thermochromic reversibility characteristic of P(PCDA-ABA). The high-temperature thermochromic reversibility is likely attributed to the strong and synergistic intermolecular hydrogen-bonding interactions within the P(PCDA-ABA) rosettes. These interactions ensure the rigidity of the columnar rosette structure and provide robustness, serving as the driving forces for the recovery of the initial structural arrangement, even after heat-induced structural strain (blue phase).

We further investigated the effect of pH on the color transitions and the associated hydrogen-bonding behavior. Since the self-assembly process is strongly governed by hydrogen-bonding interactions, variations in pH are expected to significantly influence the supramolecular organization. Under acidic and basic conditions, distinctly different colors were clearly visible, indicating that protonation and deprotonation processes regulate the hydrogen-bonding network and consequently trigger the colorimetric response in P(PCDA-ABA). A distinct blue-to-red color transition was observed, accompanied by corresponding changes in the UV–Vis spectra, at basic pH 12 (Fig. S8). Moreover, the pH-induced color transitions were found to be reversible between pH 1 and pH 13 (Fig. S9). Upon alternating between acidic and basic conditions, the original color was nearly restored, demonstrating good reversibility. UV-vis and FT-IR spectroscopy analyses further confirmed the reversibility (Fig. S9a and S9b). In the FT-IR spectra (Fig. S9b), the hydrogen-bonded carbonyl (C═O) stretching peak at 1768 cm^{-1} and the non-hydrogen-bonded carbonyl (C═O) stretching peak at 1642 cm^{-1} disappeared upon deprotonation, likely due to enolate formation under basic conditions. Additionally, the hydrogen-bonded carbonyl (C═O) stretching peak at 1660 cm^{-1} shifted slightly to a higher frequency (1664 cm^{-1}) at pH 13. Furthermore, the N–H stretching vibration at 3272 cm^{-1} split into two distinct peaks at 3283 and 3255 cm^{-1} under basic conditions, suggesting disruption of intermolecular hydrogen bonding. Upon reprotonation, the frequency shifts observed under basic conditions nearly recovered to their original positions, indicating that the structural changes are reversible. These results suggest that basic pH induces disruption of the self-assembled state through weakening or partial disruption of hydrogen-bonding interactions.

3. Conclusion

In the present study, we have developed colorimetric polydiacetylene (PDA) rosettes exhibiting enhanced structural rigidity and reversible thermochromic behavior. A linear barbituric acid-functionalized diacetylene monomer, PCDA-ABA, was synthesized. PCDA-ABA possesses two key structural features: (i) a barbituric acid headgroup that offers multiple hydrogen-bond donor and acceptor sites, facilitating a robust hydrogen-bonding network, and (ii) a diacetylene core that enables π–π stacking interactions, promoting organized molecular assem-

bly. This cooperative non-covalent interaction drives the self-assembly of the monomers into hexameric rosette structures. These rosettes further organize into twisted, slip-stacked supramolecular columnar assemblies, stabilized by intermolecular hydrogen bonding between amide groups and π–π stacking among diacetylene. The self-assembly of PCDA-ABA in a THF : ethanol mixture at a ratio of 1 : 12 (v/v) with a concentration of 10 mg mL^{-1} afforded highly ordered twisted nanohelices. FT-IR spectroscopy revealed that the self-assembly process is mainly directed by hydrogen bonding interactions. The morphological features of the rosette-based nanohelices were characterized by SEM and TEM. TEM images revealed the presence of both isolated individual nanohelices and densely packed bundles of aggregated fibers. Furthermore, AFM micrographs provided further confirmation of the helical morphology, supporting the existence of a hierarchical assembly mechanism involving rosette-based supramolecular strands. Powder X-ray diffraction (PXRD) analysis provided detailed insights into the molecular packing patterns, further confirming the formation of the hexad rosette morphology.

The columnar stacks of PCDA-ABA hexameric rosettes were covalently cross-linked *via* UV-induced topochemical polymerization, resulting in the formation of a blue-phase PDA with enhanced rigidity and structural stability. The resulting polymeric blue-phase P(PCDA-ABA) exhibited good colorimetric property of reversible thermochromic properties upon heating up to 180 °C. The effect of pH on the self-assembled PDA was studied and showed a reversible color change. At pH 13, deprotonation causes a blue-to-red transition, and the original blue color nearly recovered upon reprotonation. This study presents an interesting approach for integrating a diacetylene template with hydrogen-bonding motifs to construct higher-order and complex supramolecular self-assemblies, which can be transformed into rigid polymeric structures complemented with colorimetric properties, exhibiting enhanced structural and functional properties.

Author contributions

Hyemin Kang: investigation, methodology, data curation, formal analysis. Woomin Jeong: investigation, methodology, data curation, formal analysis. Mohammed Iqbal Khazi: project supervision, data curation, and writing. Jong-Man Kim: conceptualization, funding acquisition, supervision, and review & editing.

Conflicts of interest

There are no conflicts to declare.

Data availability

The data supporting this article have been included as part of the supplementary information (SI). Supplementary information file contains supporting experimental details, including materials and methods and additional data. It includes details on the synthesis of PCDA-ABA, SEM images of the different morphologies of PCDA-ABA at varying THF: ethanol polarity ratios, the colorimetric response of P(PCDA-ABA) over a pH range of 1–14, and the reversible colorimetric response of P(PCDA-ABA) upon modulating pH between 1 and 13. Supplementary information is available. See DOI: https://doi.org/10.1039/d5nr04836b.

Acknowledgements

This study was supported financially by the grant from the National Research Foundation of Korea (RS-2021-NR059134 and RS-2021-NR057310).

References

1 E. Busseron, Y. Ruff, E. Moulin and N. Giuseppone, *Nanoscale*, 2013, **5**, 7098–7140.
2 Lalhruaizela, Zothansiama, Lalfakawmi, B. N. Marak, B. Hazarika, R. Kataria, N. S. Kumar, B. S. Sran and V. P. Singh, *ChemPlusChem*, 2023, **88**, e202200444.
3 M. L. Mason, T. Lin, J. J. Linville and J. R. Parquette, *Nanoscale*, 2022, **14**, 4531–4537.
4 A. Sikder, Y. Xie, M. Thomas, M. J. Derry and R. K. O'Reilly, *Nanoscale*, 2021, **13**, 20111–20118.
5 H. Zhao, S. Zhang, S. Li, X. Song, W. Liu, B. Liu and M. Dong, *RSC Adv.*, 2015, **5**, 103316–103320.
6 H. Cheng, R. Liu, R. Zhang, L. Huang and Q. Yuan, *Nanoscale Adv.*, 2023, **5**, 2394–2412.
7 Y. Cho, T. Christoff-Tempesta, S. J. Kaser and J. H. Ortony, *Soft Matter*, 2021, **17**, 5850–5863.
8 A. J. Savyasachi, O. Kotova, S. Shanmugaraju, S. J. Bradberry, G. M. Ó'Máille and T. Gunnlaugsson, *Chem*, 2017, **3**, 764–811.
9 Y. Sun, W. Zhang, B. Wang, X. Xu, J. Chou, O. Shimoni, A. T. Ung and D. Jin, *Chem. Commun.*, 2018, **54**, 3851–3854.
10 H. X. Wang, L. Xu, X. Zhu, C. Xue, L. Zhang and M. Liu, *Nanoscale*, 2022, **14**, 1001–1007.
11 J. L. Zhang, X. Ye, C. Gu, C. Han, S. Sun, L. Wang and W. Chen, *Surf. Sci. Rep.*, 2020, **75**, 100481.
12 Y. Gao, C. Berciu, Y. Kuang, J. Shi, D. Nicastro and B. Xu, *ACS Nano*, 2013, **7**, 9055–9063.
13 J. Gonzalez, I. Usabiaga, P. F. Arnaiz, I. Leon, R. Martinez, J. Millan and J. A. Fernandez, *Phys. Chem. Chem. Phys.*, 2017, **19**, 8826–8834.
14 R. Tajima, S. Nakagawa and N. Yoshie, *Polym. J.*, 2026, **58**, 1–13.
15 K. C. Hunter, L. R. Rutledge and S. D. Wetmore, *J. Phys. Chem. A*, 2005, **109**, 9554–9562.
16 T. Hirayama, A. Kumar, K. Takada and T. Kaneko, *ACS Omega*, 2020, **5**, 2187–2195.

17 I. Insua, J. Bergueiro, A. Mendez-Ardoy, I. Lostale-Seijo and J. Montenegro, *Chem. Sci.*, 2022, **13**, 3057–3068.
18 H. Lee, M. I. Khazi, D. Jang, N. N. Kadamannil, R. Jelinek and J.-M. Kim, *Langmuir*, 2025, **41**, 7824–7834.
19 L. Li, R. Sun and R. Zheng, *Mater. Des.*, 2021, **197**, 109209.
20 M. J. Seo, J. Song, C. Kantha, M. I. Khazi, U. Kundapur, J. M. Heo and J.-M. Kim, *Langmuir*, 2018, **34**, 8365–8373.
21 R. Gutzler, T. Sirtl, J. F. Dienstmaier, K. Mahata, W. M. Heckl, M. Schmittel and M. Lackinger, *J. Am. Chem. Soc.*, 2010, **132**, 5084–5090.
22 X. Gong, L. Shuai, R. L. Beingessner, T. Yamazaki, J. Shen, M. Kuehne, K. Jones, H. Fenniri and M. S. Strano, *Small*, 2022, **18**, 2104951.
23 C. Otsuka, S. Takahashi, A. Isobe, T. Saito, T. Aizawa, R. Tsuchida, S. Yamashita, K. Harano, H. Hanayama, N. Shimizu, H. Takagi, R. Haruki, L. Liu, M. J. Hollamby, T. Ohkubo and S. Yagai, *J. Am. Chem. Soc.*, 2023, **145**, 22563–22576.
24 P. Jonkheijm, A. Miura, M. Zdanowska, F. J. Hoeben, S. De Feyter, A. P. Schenning, F. C. De Schryver and E. W. Meijer, *Angew. Chem., Int. Ed.*, 2004, **43**, 74–78.
25 T. Li, D. Niu, L. Ji, Q. Li, B. Guan, H. Wang, G. Ouyang and M. Liu, *Nat. Commun.*, 2025, **16**, 1698.
26 G. Q. Yin, H. Wang, X. Q. Wang, B. Song, L. J. Chen, L. Wang, X. Q. Hao, H. B. Yang and X. Li, *Nat. Commun.*, 2018, **9**, 567.
27 N. Ahmadi, D. Y. Kim, S. S. Shin, S. Daradmare, J.-M. Kim and B. J. Park, *Small Struct.*, 2024, **6**, 2400340.
28 A. Alam and C. Xiang, *ACS Omega*, 2025, **10**, 12346–12356.
29 S. Hussain, R. Deb, S. Suklabaidya, D. Bhattacharjee and S. Arshad Hussain, *Mater. Today: Proc.*, 2022, **65**, 2765–2772.
30 C. C. Revadekar, S. S. Shin, J.-M. Kim and B. J. Park, *Small Struct.*, 2025, **6**, 2400554.
31 T. A. Villarreal, S. R. Russell, J. J. Bang, J. K. Patterson and S. A. Claridge, *J. Am. Chem. Soc.*, 2017, **139**, 11973–11979.
32 Z. Yu, C. MuYu, H. Xu, J. Zhao and G. Yang, *Polym. Chem.*, 2023, **14**, 2266–2290.
33 N. Ono, R. Seishima, K. Shigeta, K. Okabayashi, H. Imai, S. Fujii and Y. Oaki, *Small*, 2024, **20**, 2400938.
34 S. Goyal, D. Sharma, A. Deep, K. Kumar and A. L. Sharma, *ACS Appl. Polym. Mater.*, 2024, **6**, 4186–4194.
35 N. N. Kadamannil, J. M. Heo, D. Jang, R. Zalk, S. Kolusheva, R. Zarivach, G. A. Frank, J.-M. Kim and R. Jelinek, *J. Am. Chem. Soc.*, 2022, **144**, 17889–17896.
36 B. Kim, M. I. Khazi and J.-M. Kim, *Macromolecules*, 2021, **54**, 8220–8228.
37 D. Seo, T. C. Major, D. H. Kang, S. Seo, K. Lee, R. H. Bartlett and J. Kim, *ACS Sens.*, 2021, **6**, 3170–3175.
38 J. Seo, M. I. Khazi, K. Bae and J.-M. Kim, *Small*, 2023, **19**, e2206428.
39 T. K. Won, S. Y. Lee, S. H. Back, C. Cui and D. J. Ahn, *Nano Lett.*, 2025, **25**, 5529–5538.
40 Q. Xu, S. Lee, Y. Cho, M. H. Kim, J. Bouffard and J. Yoon, *J. Am. Chem. Soc.*, 2013, **135**, 17751–17754.
41 J. Zheng, J. Chen, M. Galluzzi, Y. Hou and K. Sugihara, *Nano Lett.*, 2025, **25**, 7307–7316.
42 K. Aratsu, R. Takeya, B. R. Pauw, M. J. Hollamby, Y. Kitamoto, N. Shimizu, H. Takagi, R. Haruki, S. I. Adachi and S. Yagai, *Nat. Commun.*, 2020, **11**, 1623.
43 S. Yagai, M. Suzuki, X. Lin, M. Gushiken, T. Noguchi, T. Karatsu, A. Kitamura, A. Saeki, S. Seki, Y. Kikkawa, Y. Tani and K. Nakayama, *Chemistry*, 2014, **20**, 16128–16137.
44 R. S. Johnson, T. Yamazaki, A. Kovalenko and H. Fenniri, *J. Am. Chem. Soc.*, 2007, **129**, 5735–5743.
45 S. J. Parkinson, S. D. P. Fielden, M. Thomas, A. J. Miller, P. D. Topham, M. J. Derry and R. K. O'Reilly, *Biomacromolecules*, 2024, **25**, 4905–4912.
46 A. H. Manayia, F. B. Ilhami, A. W. Lee and C. C. Cheng, *Biomacromolecules*, 2021, **22**, 5307–5318.
47 A. Isobe, T. Kajitani and S. Yagai, *Angew. Chem., Int. Ed.*, 2023, **62**, e202312516.
48 M. Okuno, S. Yamada, T. Ohto, H. Tada, W. Nakanishi, K. Ariga and T. A. Ishibashi, *J. Phys. Chem. Lett.*, 2020, **11**, 2422–2429.
49 F. Silly, M. Kawaura, T. Aizawa, H. Ouchi and S. Yagai, *J. Phys. Chem. C*, 2022, **126**, 2780–2787.
50 S. Yao, R. Brahmi, F. Portier, J. L. Putaux, J. Chen and S. Halila, *Chemistry*, 2021, **27**, 16716–16721.
51 C.-C. Chu, G. Raffy, D. Ray, A. D. Guerzo, B. Kauffmann, G. Wantz, L. Hirsch and D. M. Bassani, *J. Am. Chem. Soc.*, 2010, **132**, 12717–12723.
52 R. I. Andina, S. Kingchok, K. Laohhasurayotin, N. Traiphol and R. Traiphol, *Colloids Surf., A*, 2022, **647**, 129117.
53 C. Song, J. Huang, C. Qiu and Y. Yang, *React. Funct. Polym.*, 2025, **215**, 106357.
54 S. Baek, J. M. Heo, K. Bae, M. I. Khazi, S. Lee, K. Kim and J.-M. Kim, *Langmuir*, 2024, **40**, 18272–18282.
55 W. Jeong, M. I. Khazi, D. G. Lee and J.-M. Kim, *Macromolecules*, 2018, **51**, 10312–10322.
56 H. Xing, Y. Song, L. Ma, F. Wang, M. Zhang, Z. Li, Z. Wan, X. Cui and G. Yang, *ACS Appl. Polym. Mater.*, 2024, **6**, 15035–15042.
57 C. Qiu, X. Zhang, C. Song and Y. Yang, *Langmuir*, 2025, **41**, 25716–25728.
58 M. Bruschi, P. A. Limacher, J. Hutter and H. P. Lüthi, *J. Chem. Theory Comput.*, 2009, **5**, 506–514.
59 W. Jeong, M. I. Khazi, D. G. Lee and J.-M. Kim, *Macromolecules*, 2018, **51**, 10312–10322.
60 I. S. Park, H. J. Park, W. Jeong, J. Nam, Y. Kang, K. Shin, H. Chung and J.-M. Kim, *Macromolecules*, 2016, **49**, 1270–1278.